METEOROLOGICAL APPLICATIONS
Meteorol. Appl. (2008)
Published online in Wiley InterScience
(www.interscience.wiley.com) DOI: 10.1002/met.111

Assessing the diurnal evolution of surface radiation balance over the western region of Tropical Atlantic Ocean using *in situ* measurements carried out during the FluTuA Project

Sarasvati Bacellar,[a] Amauri P. Oliveira,[a,*] Jacyra Soares[a] and Jacques Servain[b†]
[a] *Department of Atmospheric Sciences, University of São Paulo, Brazil*
[b] *Institut de Recherche pour le Développement (IRD), UMR-182, Paris, France.*

ABSTRACT: In this work, the diurnal evolution of the radiation balance components over the tropical Atlantic Ocean is described and analysed. The analysis is based on measurements carried out on board a Brazilian Navy ship during the observational campaign of the FluTuA Project ('Fluxos Turbulentos sobre o Atlântico'), from 15 to 23 May 2002. The observations indicated that the albedo responds as expected to atmospheric attenuation effects with a diurnal evolution similar to the Fresnel albedo. In general, the observed longwave radiation values agreed better with the estimated values obtained without longwave reflection. In agreement with the literature, the average surface emissivity was around 0.97. The net radiation, estimated from published equations for albedo, atmospheric transmissivity and surface emissivity, agreed with the observations, indicating that these parameters are representative of the radiometric properties of the air-sea interface in the region between Natal (6 °S, 35.2 °W) and the São Pedro and São Paulo Archipelago (1 °N, 29.3 °W).

KEY WORDS albedo; atmospheric transmissivity; surface emissivity; air-sea interaction and São Pedro and São Paulo Archipelago

Received 14 November 2007; Revised 26 June 2008; Accepted 15 September 2008

1. Introduction

Climate change issues have brought attention to the scarcity of information about the short-term variation of ocean-atmosphere interactions. Discrepancies between climate models are known worldwide and are particularly important over the tropical and subtropical regions of the South Atlantic Ocean. There, climate models diverge about the intensity of the heat, moisture and momentum fluxes between atmosphere and ocean (Wainer *et al*., 2003). To assess the uncertainty of the air–sea flux values and to improve the knowledge of the climatology of the ocean-atmosphere interaction *in situ* measurement data are necessary. However, there are very few field measurements over the South Atlantic Ocean with the time and space resolutions required to investigate the atmospheric short-term variations (Dourado and Oliveira, 2001; Pezzi *et al*., 2005).

The EQUALANT 99 programme, a component of the Etudes CLimatiques dans l'Atlantique Tropical (ECLAT) the French programme of the CLImate VARiability and predictability (CLIVAR) programme, for instance, was mainly dedicated to the study of oceanic circulation in the tropical Atlantic basin (Gouriou *et al*., 2001). It was also devoted to the estimation of surface fluxes to obtain bulk flux parameterization adapted to the mooring network in this region (the Pilot Research Moored Array in the Tropical Atlantic (PIRATA) programme; Servain *et al*., 1998). Analysis of this experiment is still in progress (Weill *et al*., 2003).

The Global Atmospheric Research Programme's (GARP) Atlantic Tropical Experiment (GATE) (Kuettner, 1974) was conducted over the north tropical Atlantic Ocean, in the summer of 1974 and, more recently, the AERosol and Ocean Science Expedition (AEROSE). The fundamental purpose of the AEROSE mission was to provide a set of critical measurements to characterize the impacts and microphysical evolution of Saharan dust aerosol transport across the Atlantic Ocean (Nalli *et al*., 2006).

The PIRATA programme maintains an array of 12 next generation Autonomous Temperature Line Acquisition System (ATLAS) buoys with the principal objective of describing and understanding the evolution of the sea surface temperature, upper ocean thermal structure and air–sea fluxes of momentum, heat and fresh water in the tropical Atlantic. The oceanic and meteorological observations are transmitted to ground station *via* satellite by Service Argos and are available in near real-time on the internet (http://www.pmel.noaa.gov/pirata).

Solar radiation is the primary energy source for the atmospheric general circulation and the hydrological

† Current affiliation: FUNCEME, Fortaleza, CE, Brazil.
* Correspondence to: Amauri P. Oliveira, Departamento de Ciencias Atmosfericas – IAG-USP, Rua do Matao, 1226, Sao Paulo, SP, 05508-090, Brazil. E-mail: apdolive@usp.br

cycle. The coupling between atmospheric and oceanic general circulation models depends strongly on the radiative energy flux through the Earth-atmosphere system. For the radiative energy balance near the surface the shortwave solar energy accounts for most of the heat flux transferred to the ocean. The solar radiation transferred into the upper-ocean layers affects the stability of the ocean mixed layer and the sea surface temperature. Consequently, the oceanic surface albedo plays a key role in determining the energy flux exchanged between atmosphere and ocean and so it is an important issue for the coupling of atmosphere and ocean models (Li *et al*., 2006).

An exact knowledge of the components of the radiation balance is also very important in both climate and weather forecasting. Changes in the radiation balance can lead to climate changes and because of that it is interesting to monitor those balance components.

The present work describes the *in situ* radiation observations obtained during 15–23 May 2002, as part of the FluTuA Programme (Soares *et al*., 2001). These observations were carried out on board the Brazilian Navy Ship *Comte Manhães*, between Natal (6 °S, 35.2 °W) and the São Pedro and São Paulo Archipelago, approximately 1100 km off the coast of Brazil (1 °N, 29.3 °W), passing by the Fernando de Noronha Archipelago (3.8 °S, 32.4 °W) (Figure 1).

The FluTuA Programme intends to measure turbulent fluxes at the atmospheric surface layer and vertical profiles of meteorological and oceanographic parameters over the western tropical Atlantic Ocean. The major goals were to characterize observationally the interaction between the atmosphere and the ocean on the micro, meso and macro scales. The surface boundary layer fluxes were determined from an instrumented tower located on the SPSPA.

Very little is known about the atmospheric and oceanographic conditions in the SPSPA region. During 1983–1984, *in situ* wind measurements were collected at SPSPA, as part of Francais Océan Climate Atlantique Equatorial/Seasonal Equatorial Atlantic Experiment (FOCAL/SEQUAL) experiment. The wind velocity showed a decrease in the periods from February through April in 1983 and from January through May in 1984. From April through November 1983 and from May to the end of October 1984, wind velocities were practically constant, with a mean velocity of about 6.9 m s^{-1} in 1983 and 6 m s^{-1} in 1984 (Colin and Garzoli, 1987). The wind decrease is associated with the seasonality and positioning of the Intertropical Convergence Zone (ITCZ). From February to April the winds became very weak because the low wind confluence zone was positioned over the SPSPA in 1983. According to Wainer and Soares (1997), the sea surface temperature in the tropical Atlantic is in phase with the meridional displacement of the ITCZ and out of phase with rainfall in north-northeast Brazil.

This work compares the diurnal evolution of radiometric properties of the atmosphere (broad band transmissivity) and surface (albedo, emissivity and net longwave radiation) with general formulations, tested for open ocean conditions at tropical latitudes, available in the literature (WGASF, 2001). The *in situ* observations and the correction used for the solar heating effects on the longwave radiation are described in Section 2. The main results are displayed in Section 3 and the discussions and conclusions are in Section 4.

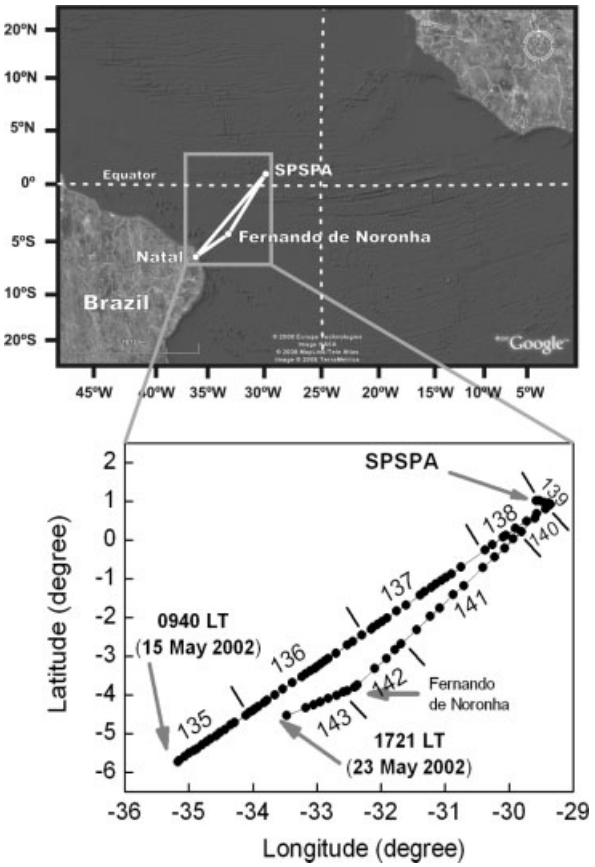

Figure 1. Trajectory described by Comte Manhães during the observational campaign of FluTuA project and the geographic position of Natal, Fernando de Noronha and São Pedro e São Paulo Archipelago (SPSPA). Geographic position of the ship during the observational campaign, carried out between 15 and 23 May 2002. The ship left Natal on 15 May at 0940 local time (LT) and arrived at São Pedro and São Paulo Archipelago (SPSPA) on 19 May at 1025 LT. On 20 May at 1940 LT the ship left SPSPA and arrived in Fernando de Noronha on 22 May at 1150 LT and left on 23 May at 0910 LT (LT = UTC − 3).

2. Observations

The observations were carried out on board of the Brazilian Navy ship *Comte Manhães*. The ship was set up with wind velocity, air temperature, air relative humidity, radiation, and water temperature sensors. The characteristics of the sensors are described in Table I. The water temperature sensor was protected from direct solar radiation and measured the water temperature at 1 m depth. According to Kurzeja *et al*. (2005) the measurements of water temperature correspond to the bulk sea surface temperature (SST). The bulk layer is between 1 and 5 m deep and is sampled by ships and buoys. In this experiment, the bulk SST observations

DOI: 10.1002/met

Table I. Sensor characteristics.

Sensor	Manufacturer	Accuracy	Response time at 95% (s)
Net Radiometer, model CNR1	Kipp and Zonen	2.5%	18
Anemometer Gill Propeller	R.M. Young	1 m s^{-1}	–
Air temperature	Vaisala	0.2 °C	–
Air relative humidity	Vaisala	4%	15
Water temperature	Vaisala	0.2 °C	–

were periodically compared with the water temperature collected using a bucket (not shown here). All the sensors were connected to the data acquisition system Datalogger 21X, manufactured by Campbell Inc. The sampling rate was set equal to 0.2 Hz and the 5-min average was calculated for all variables.

The net radiation sensor was arranged in the up front of the vessel, about 1 m from the ship, and 6 m above the sea surface. The net radiation sensor was fixed in respect to the ship and no compensation was carried out for the ship movement. The air temperature and relative humidity sensors were mounted at the upper level of the ship, near to the wind sensors, at 11 m above the sea surface. Two anemometers were set up in the boom located at the upper level of the ship, also 11 m above the sea surface. The anemometers were oriented in the directions parallel and perpendicular to the ship.

The performance of the four radiation sensors, forming the model CNR1 net radiometer manufactured by Kipp-Zonen Inc., were, prior to and after the campaign, individually compared with a PSP pyranometer (shortwave sensor) and PIR pyrgeometer (longwave sensor), both manufactured by Eppley Lab Inc. The Kipp-Zonen net radiometer and Eppley radiometers were set side-by-side measuring incoming solar and atmospheric radiation at the surface during few days. Information about Eppley sensors and calibration procedure can be found in Oliveira *et al*. (2006). The results (not shown here) indicated an agreement compatible with the accuracy provided by the manufacturer (Table I). Similar performance tests were carried out for the other sensors used in the observational campaign (Table I).

The solar heating effects on the performance of the longwave radiation sensor were corrected using the equation proposed by Pérez and Alados-Arboledas (1999):

$$LW^{\mathrm{Cor}} = LW^{\mathrm{Obs}} - [0.033 + 0.015\ exp(-V/3.2)]\ SW_{\mathrm{DW}}. \quad (1)$$

Here it was assumed that $V = \sqrt{u^2_{\mathrm{air-ship}} + v^2_{\mathrm{air-ship}}}$ is the absolute value of the wind velocity in respect to the ship (m s^{-1}), LW^{Obs} corresponds to the observed values of longwave radiation emitted by the atmosphere or by the surface and SW_{DW} is the incoming solar radiation at the surface.

Equation (1) was derived originally for direct horizontal solar radiation, however, as pointed out by Pérez and Alados-Arboledas (1999) it can also be applied using global solar radiation. This equation was also developed exclusively to correct dome emission effects in pyrgeometer model PIR manufactured by Eppley Inc., which has a bulged dome. The Kipp-Zonen longwave radiation sensors are a CG3 model having a flat dome. Even though the internal circuitry compensates heating effects on longwave radiation measurements, it will be shown in next sections that the pronounced diurnal cycle in both upward and downward longwave radiation was eliminated when Equation (1) was applied.

The ship's position and trajectory (Figure 1) were obtained from an onboard GPS system. This information was also used to estimate the ship velocity and direction. The ship direction corresponds to the angle formed between the ship and north, analogous to the horizontal wind direction angle in meteorological convention. The wind velocity and direction were estimated using the wind velocity components measured on board the ship and considered that the ship was in a straight line between two consecutive GPS positions.

Most of the time the measurements were performed at open-ocean conditions where the air temperature was higher than the sea surface temperature. Only near the continent (at the very beginning of the experiment, shown as number 1 in Figure 2(a)) and near the Fernando de Noronha Archipelago (shown as number 3 in the figure) was the air temperature lower than the sea surface temperature. It is interesting to note that near the SPSPA (number 2 in Figure 2(a)) the environment behaves like an open ocean. The SPSPA is an outcrop of the mid-Atlantic Ridge; its largest island has an area of approximately 7500 m^2 with the highest point at 17 m. Therefore, the geographical location and low topographic features of SPSPA characterize this site as an ideal place to measure unobstructed weather parameters under open ocean conditions. The air and water temperatures are also shown in Figure 2(b) for year day 136.

The actual Sun position at different longitudes occupied by the ship during the trip was taken into consideration in the estimate of the extraterrestrial solar radiation. All measurements and estimates were reported in terms of the local time of Natal (6 °S, 35.2 °W) which corresponds to the Brazilian standard time (= UTC − 3). In this work, all radiation fluxes are positive when oriented upward and *vice versa*.

DOI: 10.1002/met

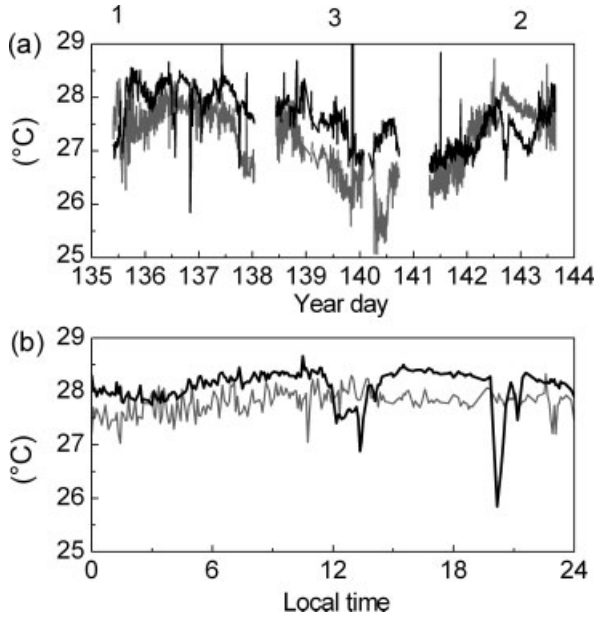

Figure 2. Time evolution of air (black line) and surface water temperatures (grey line) observed during whole experiment and (b) year day 136 of 2002. In (a) the numbers correspond, respectively, to when the ship left the continent, arrived at the SPSPA and arrived at the Fernando de Noronha.

3. Results

Here will be shown the radiometric properties (surface emissivity, net sky transmissivity and surface albedo) of the region and the net radiation at the surface.

3.1. Surface emissivity

Over the ocean, the longwave radiation emitted by the atmosphere (LW_{DW}) can be estimated as (Clark *et al*., 1974):

$$LW_{\mathrm{DW}} = \left(R_{\mathrm{N}}^{\mathrm{LW}} - \varepsilon_0 \sigma \ {T_{\mathrm{S}}}^4\right) / (1 - \alpha_{\mathrm{LW}}), \qquad (2)$$

where $R_{\mathrm{N}}^{\mathrm{LW}}$ is the net longwave radiation at the surface, ε_0 is the surface emissivity assumed equal to 0.98, σ is the Stefan-Boltzman constant, T_{S} is the surface temperature measured with the thermistor dropped in the water (Figure 2) and α_{LW} is the longwave radiation reflectivity of the surface set equal to 0.045 (Josey *et al*., 1997).

Clark *et al*. (1974) gave an empirical equation to estimate the net longwave radiation over open ocean conditions:

$$R_{\mathrm{N}}^{\mathrm{LW}} = \left(a - b\sqrt{e_A}\right) \ \varepsilon_0 \sigma \ {T_{\mathrm{S}}}^4 \ (1 - \lambda \ n^2) + 4 \ \varepsilon_0 \ \sigma {T_{\mathrm{S}}}^3 (T_{\mathrm{S}} - T_{\mathrm{A}}), \qquad (3)$$

where e_{A} is the vapour pressure value in mb, T_{A} is the air temperature measured on board of ship at 11 m above the sea level (Figure 2), a and b are empirical constants set equal to 0.39 and 0.05 respectively (Josey *et al*., 1997) and n is the fractional cloud cover in oktas. The latitude dependent cloud cover coefficient, λ, assumes the value of 0.51 at the equator (Clark *et al*., 1974). The vapour pressure, used in Equation (3), was estimated using observed relative humidity of the air at 11 m and considering the atmospheric pressure constant and equal to 1010 hPa (the averaged value obtained by the ship's barograph).

Figure 3 displays the observed and estimated values of $R_{\mathrm{N}}^{\mathrm{LW}}$. The match between the observed values (grey circles in the figure) and the estimated values improves with the specification of a fractional cloud cover. Here n was set equal to 2 oktas (the continuous line in Figure 3) because some clouds were often present during short periods, affecting the net longwave radiation even when the atmospheric transmissivity was high (Section 3.2).

The observed values of LW_{DW}, corrected by Equation (1) and without correction, are displayed in Figure 4, together with the estimated values of LW_{DW} with α_{LW} equal to 0.0. Using the estimated values as reference (the continuous line in Figure 4) it is possible to verify that the diurnal oscillations present in the observed values of LW_{DW} are not related to the diurnal cycle of the surface and air temperatures (Figure 2(b)) but they are related to the solar heating effects on the radiation sensor (Pérez and Alados-Arboledas, 1999; Weller *et al*., 2004).

The diurnal evolution of the atmospheric downward longwave radiation estimated using Equation (2) and corrected using Equation (1) is indicated in Figure 5. The

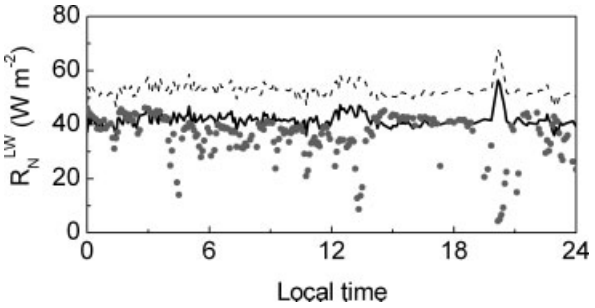

Figure 3. Diurnal evolution of the observed net longwave radiation on year day 136. The grey solid circles show the observed values; the dashed line the $R^{\mathrm{LW}}{}_{\mathrm{N}}$ estimated considering no clouds and the continuous line the values estimated considering a fractional cloud cover of 2 oktas.

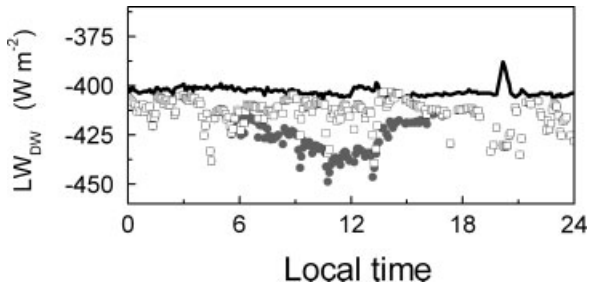

Figure 4. Diurnal evolution of the observed longwave radiation emitted by the atmosphere without correction (grey solid circles) and with correction based on Pérez and Alados-Arboledas (1999) (open black squares) on year day 136. The continuous line corresponds to the estimated values of LW_{DW} using α_{LW} equal to 0.0.

DOI: 10.1002/met

observed LW_{DW} emission, at 6 m, is within the estimated LW_{DW} using α_{LW} equal to zero (thin line in Figure 5) and α_{LW} equal to 0.045 (thick line in Figure 5). The estimated LW_{DW} emission reproduced the observation regardless the value of α_{LW}. A more conclusive figure about the role of longwave radiation reflection at the surface will be shown next.

The outgoing longwave radiation from the surface (LW_{UP}) corresponds to the emission from the surface plus the downward atmospheric emission reflected upwards by the surface:

$$LW_{UP} = \varepsilon_0 \sigma T_S^4 - \alpha_{LW}\ LW_{DW}. \qquad (4)$$

Figure 6 shows the diurnal evolution of the observed and estimated values of LW_{UP}, using Equation (4) and corrected by Equation (1). Similarly to LW_{DW} the diurnal oscillations present in the observed values of LW_{UP} are not related to the diurnal cycle of the surface and air temperatures because they didn't show any significant variation during daytime (Figure 2(b)). However, they can be related to the solar heating effects on the radiation sensor. A similar solar heating effect was detected in the TOGA-CORE experiment and removed from the longwave radiation atmospheric emission using a different method but with similar outcome (Weller *et al*., 2004).

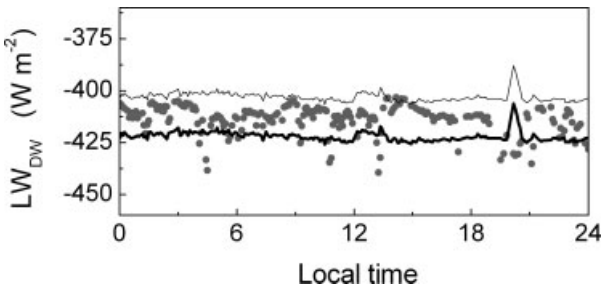

Figure 5. Diurnal evolution of the corrected observed (grey solid circles) and estimated (continuous line) longwave radiation emitted by the atmosphere on year day 136. The thick and thin continuous lines correspond, respectively, to the estimated values of LW_{DW} using α_{LW} equal to 0.045 and 0.0.

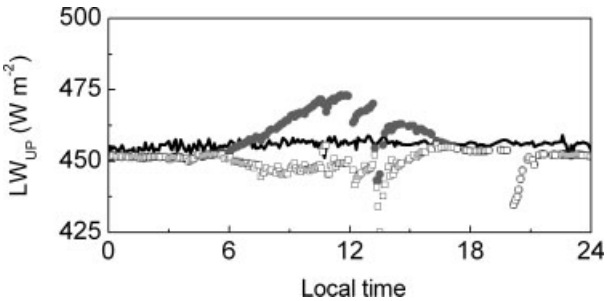

Figure 6. Diurnal evolution of the observed longwave radiation emitted by the ocean surface without correction (grey solid circles) and with correction based on Pérez and Alados-Arboledas (1999) (open black squares) on year day 136. The continuous line corresponds to the estimated values of LW_{UP} using α_{LW} equal to 0.0.

The best match between the estimated and observed values of the longwave radiation emitted by the surface is obtained when the LW_{UP} values are estimated without considering the longwave reflection of the surface (thin line in Figure 7).

The corrected values of surface longwave radiation emission were used to estimate the emissivity of the surface (ε_{OBS}), following the equation:

$$\varepsilon_{OBS} = \left(LW_{UP}^{Cor} - \alpha_{LW}\ LW_{DW}^{Cor}\right) / \sigma T_S{}^4. \qquad (5)$$

The frequency of the surface emissivity values (Figure 8) shows that the most probable value of surface emissivity is 0.97. This value, obtained using Equation (5) and $\alpha_{LW} = 0$, is consistent with the surface emissivity 0.98 used in net longwave radiation bulk formula. Recent observations have indicated similar surface emissivity over tropical open ocean conditions (Bhat *et al*., 2003). The observed value also agrees with the emissivity observed by Smith *et al*. (1996) between 8 and 13 μm and near to nadir view.

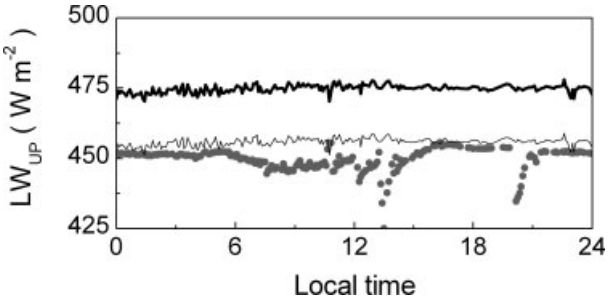

Figure 7. Diurnal evolution of the observed corrected (grey solid circles) and estimated (continuous lines) longwave radiation emitted by the ocean surface on year day 136. The thick and thin continuous lines correspond, respectively, to the estimated values of LW_{UP} using α_{LW} equal to 0.045 and 0. Corrections on observed values of LW_{UP} were based on Pérez and Alados-Arboledas (1999).

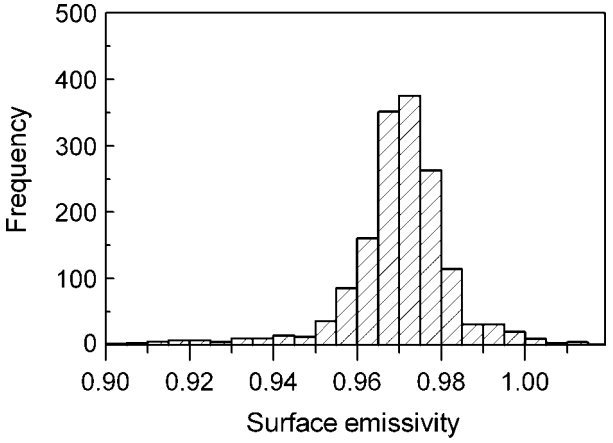

Figure 8. Frequency distribution of the surface emissivity values estimated from the observed values of LW_{UP} without reflection ($\alpha_{LW} = 0$). The highest frequency emissivity is 0.97.

DOI: 10.1002/met

3.2. Net sky transmissivity

In the absence of clouds the diurnal evolution of the net sky transmissivity (Γ) can be estimated from the following equation (Stull, 1988):

$$\Gamma = (a_\Gamma + b_\Gamma \cos\ Z), \tag{6}$$

where a_Γ and b_Γ are constants that take into consideration the clear sky depletion and Z is the solar zenith angle, defined to be the angle between the Sun and the vertical.

The broadband transmissivity of the atmosphere was obtained as $\Gamma = SW_{\mathrm{DW}}/SW^{\mathrm{T}}_{\mathrm{DW}}$, where SW_{DW} is the incoming solar radiation at the surface. The solar radiation at the top of the atmosphere $SW^{\mathrm{T}}_{\mathrm{DW}}$ was estimated using $SW^{\mathrm{T}}_{DW} = -I_0 \cos Z$, with I_0 being the solar constant given by $I_0 = S_0\left(\overline{D}/D\right)^2$, where S_0 is the average solar constant assumed equal to 1366 W m^{-2} (Frölich and Lean, 1998), $\overline{D}$ is the average distance between the Sun and the Earth, D is the actual Sun–Earth distance and Z is the solar zenith angle. The ratio $(\overline{D}/D)^2$ and Z are calculated according to Iqbal (1983).

Figure 9 displays the time variation of the sky atmospheric transmissivity observed and estimated by Equation (6) using the coefficient set derived from observed clear sky transmissivity data ($a_\Gamma = 0.5$ and $b_\Gamma = 0.3$). Unfortunately, there was no cloud observation during the expedition.

The observed and estimated incoming shortwave radiations at the surface using $\Gamma = 0.5 + 0.3\ \cos\ Z$, and the solar radiation at the top of the atmosphere, are displayed in Figure 10. Despite the unaccounted presence of clouds, the observed net sky transmissivity and, as consequence, the global solar radiation at the surface are well characterized using $\Gamma = 0.5 + 0.3\ \cos\ Z$.

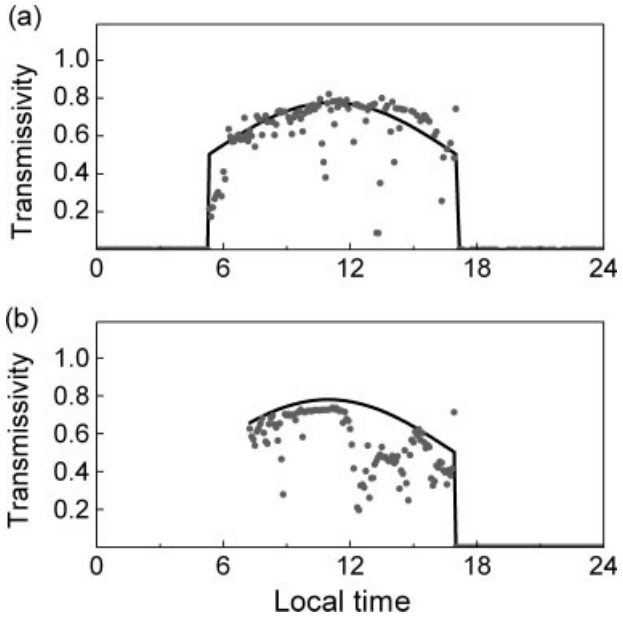

Figure 9. Diurnal evolution of the atmospheric 'net sky' transmissivity for year days (a) 136 and (b) 141 of 2002. The curve $\Gamma = 0.5 + 0.3\ \cos\ Z$ (continuous line) was interpolated through the entire data set considering the clear sky values of transmissivity only. The observed values are displayed as grey solid circles.

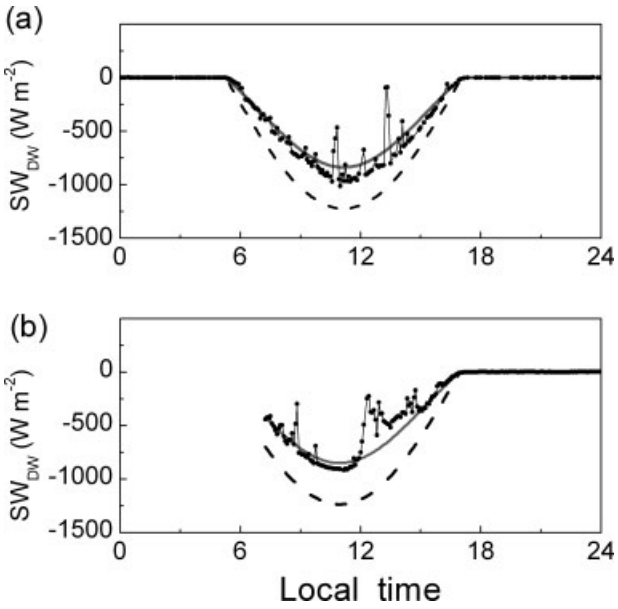

Figure 10. Diurnal evolution of the observed (line-solid circles) and estimated (continuous grey line) incoming shortwave radiations at the surface for year day (a) 136 and (b) 141 of 2002. The solar radiation at the atmospheric top is displayed in dashed line.

Li and Lam (2001) classified the sky condition, during a particular period, according to the value of Γ (or K_T, as named in their paper). They found that the sky is clear when Γ is greater than 0.7; partly cloud when $0.15 < \Gamma < 0.7$ and overcast when Γ is smaller than 0.15. For instance, considering the period investigated here (May, 2002), the minimum value of solar zenith angle was around 20°, generating a Γ value of the order of 0.78. The minimum Z for day 136 is 22.5° and the minimum Z for day 141 is 20.8° resulting in Γ values of, respectively, 0.777 and 0.781. According to Li and Lam (2001), these values can be classified as clear sky conditions. Oliveira *et al*. (2002) also found close values to clear sky conditions for polluted continental areas in Brazil.

Therefore, despite the presence of some clouds, mainly during the afternoon, most of the days are basically clear sky days. The ITCZ positions at the beginning and the end of the field campaign are located at slightly higher latitudes than the area covered by the ship (Figure 11).

The intensity of global solar radiation can be attenuated by aerosol and moisture content of the atmosphere. Dust transport from Africa can reach the tropical portion of the Atlantic Ocean (Nalli *et al*., 2006). Unfortunately, there were no measurements of air aerosol content during the FluTuA expedition. However, the transmissivity values obtained here indicate that the aerosol effects were not too strong to affect significantly the solar radiation at the surface, during the investigated period.

DOI: 10.1002/met

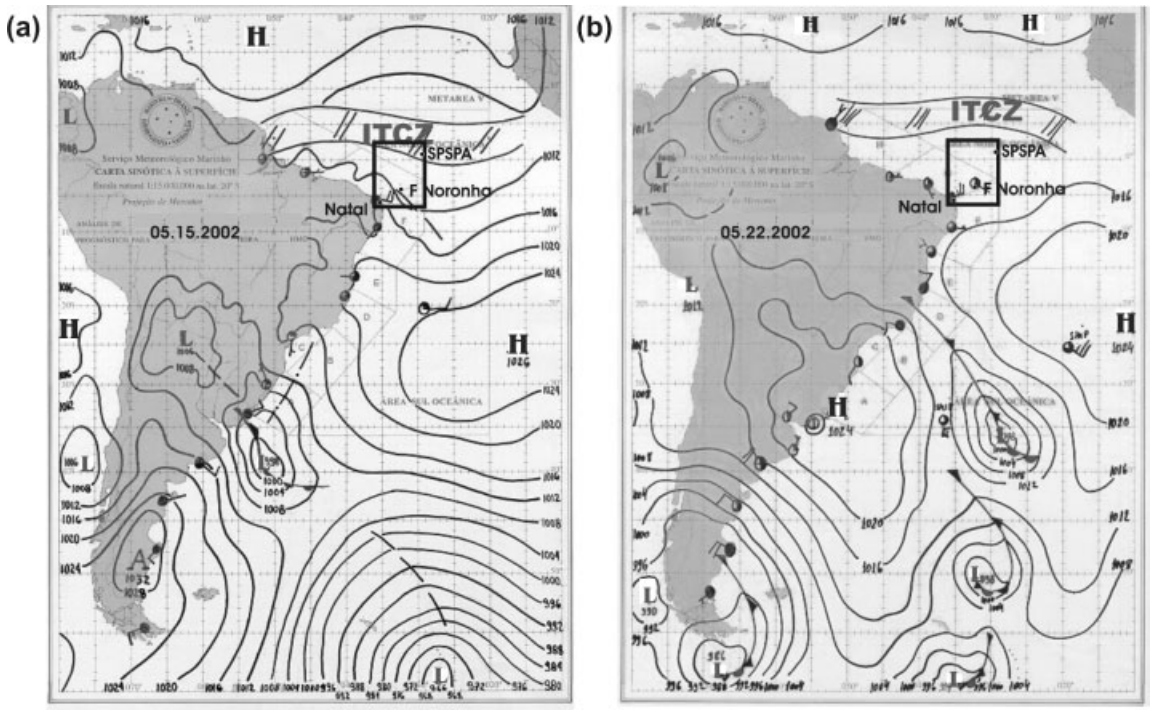

Figure 11. Surface synoptic chart at May (a) 15 and (b) 22, 2002. The ITCZ position is located in the Northern Hemisphere. The area covered by the field campaign is indicated by the rectangle.

3.3. Surface albedo

The surface albedo over the ocean (α) can be estimated from the Fresnel equation:

$$\alpha = 0.50 \left[\frac{\sin^2(Z-r)}{\sin^2(Z+r)} + \frac{\tan^2(Z-r)}{\tan^2(Z+r)} \right], \qquad (7)$$

where r is the refraction angle of the light in the water given by $r = arcsin[(\sin\ Z)/ni]$, ni is the seawater refraction index equal to 1.33. In this equation the surface of the water is considered flat and the contribution from diffuse solar radiation reflection is not included (Cogley, 1979).

According to Jin *et al.* (2004), the surface albedo is a function of the transmissivity (cloud cover, atmospheric load of aerosol and water vapour), zenith angle, ocean surface state (wind velocity) and chlorophyll water content. Payne (1972) found that the albedo does not depend on the solar zenith angle when the transmissivity values are below 0.1. On the other hand, for transmissivity between 0.60 and 0.65 the albedo shows a very well defined variation with solar zenith angle, following closely the behaviour described Equation (7).

Figure 12 shows the average surface albedo as a function of solar zenith angle, calculated from the solar radiation observations as $\alpha = -SW_{\mathrm{UP}}/SW_{\mathrm{DW}}$, where SW_{UP} is the observed outgoing solar radiation from the surface. The observed average albedo for lower zenith angles, about 0.06, is compatible with the albedo value found by Payne (1972) for conditions of light winds and relatively smooth seas, however, it disagrees with the predicted values from Equation (7). The albedo obtained by Jin *et al.* (2004), derived from 2 years of observations and considering only clear sky conditions, agreed well with the Fresnel albedo.

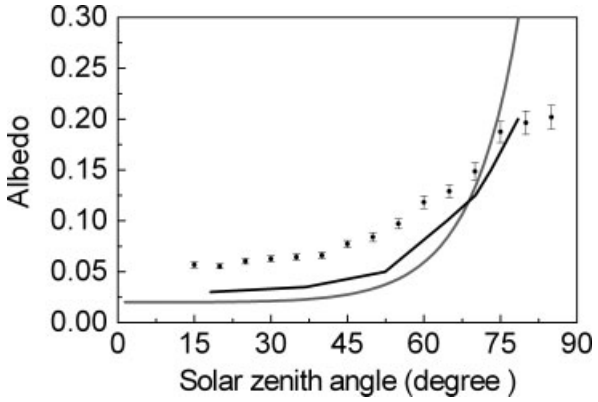

Figure 12. Average surface albedo as a function of the solar zenith angle, based on observations carried out during the entire campaign (black solid circles). The vertical bars correspond to the statistical error. The grey continuous line indicates the albedo estimated using Equation (7). The black continuous line indicates the albedo proposed by Jin *et al.* (2004).

Considering the albedo diurnal evolutions during year days 136 and 141, it can be seen that the discrepancies between the observed albedo and the albedo estimated using the Fresnel equation are more pronounced in year day 136 (Figure 13(a)) than in year day 141 (Figure 13(b)). The discrepancies on year day 136 can be caused by the anomalous larger values of albedo observed when the ship was moving from SW to NE directions, facing the Northern Hemisphere, towards the SPSPA (Figure 1). During the entire field campaign, the

DOI: 10.1002/met

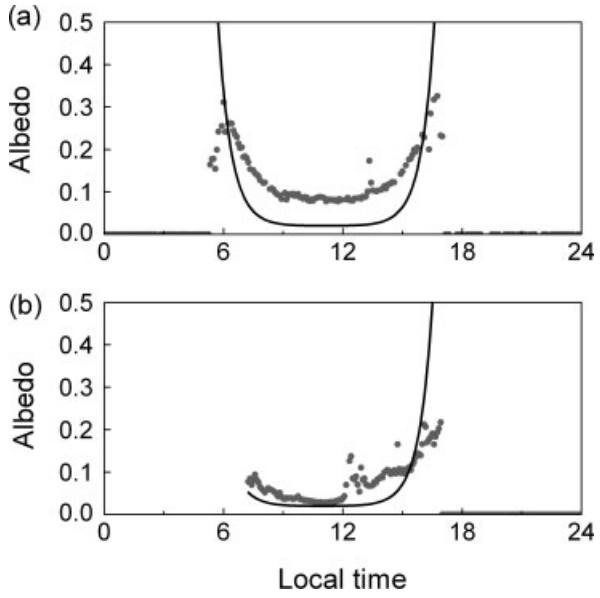

Figure 13. Diurnal evolution of the surface observed (grey solid circles) and estimated albedos (continuous line) for year day (a) 136 and (b) 141 of 2002.

Sun was in the Northern Hemisphere and therefore the incoming solar radiation reflected over the sensor positioned in the frontal part of the ship artificially increased the albedo. During the return from SPSPA the ship was facing the Southern Hemisphere and the reflection caused by the ship was not significant. The observed albedo dependence with the ship orientation can be more clearly seen in Figure 14. For all solar elevation angles, the estimated albedo, given by Equation (7), matches the observed albedo during year days 141–143, when the solar radiation sensors were not located between the ship and the Sun. The afternoon discrepancies on year day 141 can be associated to cloud cover effects, as can be seen in Figures 9(b), 10(b) and 13(b).

The ship reflection effect can also be identified considering the dependence between albedo and transmissivity.

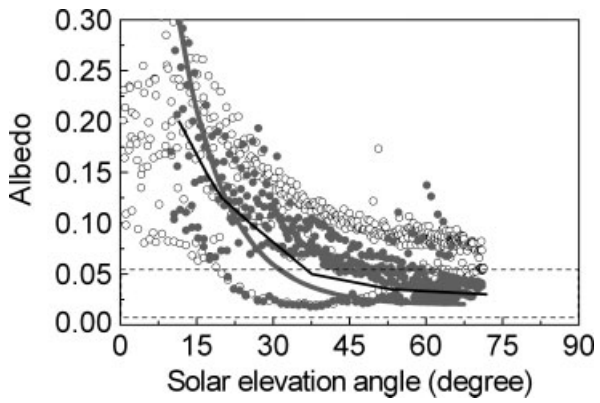

Figure 14. Albedo as a function of the solar elevation observed during year days 135–138 when the ship was facing the Northern Hemisphere (black open circles) and during year days 141–143 when the ship was facing the Southern Hemisphere (grey solid circles). Grey thick line corresponds to the albedo estimated from Fresnel equation. The black continuous line is the albedo proposed by Jin *et al.* (2004).

According to Payne (1972) and Simpson and Paulson (1979), for large transmissivity values the sea surface albedo behaves in the Fresnel manner, varying with solar elevation.

Figure 15 shows the observed albedo as a function of the solar elevation angle for different transmissivity intervals. The albedo values obtained, for mid-ocean (35 °N, 155 °W), by Simpson and Paulson (1979) are also displayed in Figure 15. For low transmissivity conditions (cloudy skies or $0 < \Gamma < 0.33$) the albedo values found by Simpson and Paulson (1979) have a smaller dependence with the sun position than the observed albedo (Figure 15(a)). For partially cloudy ($0.4 < \Gamma < 0.5$) and clear ($0.5 < \Gamma < 0.6$) sky conditions the observed albedo response to the solar elevation follows the behaviour found by Simpson and Paulson (1979). Larger discrepancies in these two last conditions are found between year days 135 and 138 (open circles in Figure 15(b), (c)) when the ship was facing the Northern Hemisphere.

Figure 16 shows the albedo as a function of the atmospheric transmissivity for two values of sun elevation (10° and 70°). The results obtained by Payne (1972) in the mouth of Buzzards Bay, USA (41.4 °N, 71.03 °W) is one of the few long term observational studies of albedo carried out on a fixed platform. The 10° and 70° Sun elevation values were estimated considering, respectively, the average albedo for Sun elevations between 5 and 15° and 65 and 75°. The observations carried during FluTuA follow Payne's (1972) prediction during the return leg (year days 141–143), when the ship was facing the Southern Hemisphere. During the expedition towards SPSPA (year days 135–138) the discrepancies are larger for a Sun elevation of 70° as a consequence of the ship reflection effects.

As expected, the behaviour of the shortwave radiation reflected by the ocean surface agrees with the estimated values when the ship was moving back from SPSPA and, therefore, facing the Southern Hemisphere (Figure 17). The largest discrepancies between the observed and estimated SW_{UP} were found during the year days 139 and 140 (not shown here) when the ship was practically not moving (Figure 1). Therefore, these days were removed from the analysis carried out for albedo and displayed in Figures (12) and (14)–(16).

3.4. Net radiation at surface

The estimated net radiation at the ocean surface (R_N) was evaluated considering the shortwave and longwave atmospheric components at the air–sea interface:

$$R_N = SW_{DW} + SW_{UP} + LW_{DW} + LW_{UP}, \qquad (8)$$

where the shortwave radiation components SW_{DW} and SW_{UP} were evaluated using the transmissivity coefficients given by Γ and the surface albedo given by Equation (7).

The daytime evolution of the difference between estimated and observed values of net solar radiation

DOI: 10.1002/met

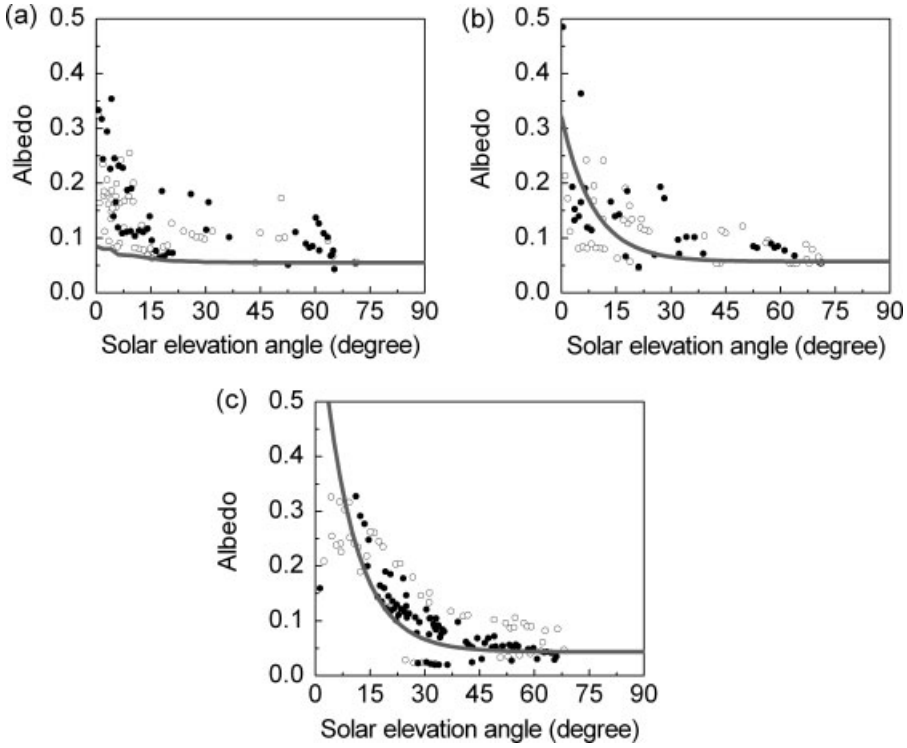

Figure 15. Albedo as a function of the solar elevation for atmospheric transmissivity between (a) 0.0 and 0.33 (b) 0.30 and 0.40 and (c) 0.50 and 0.60. Observed during year days 135–138 (open circles) and during year days 141–143 (solid circles). Grey line corresponds to the albedo proposed by Simpson and Paulson (1979) for equivalent transmissivity intervals.

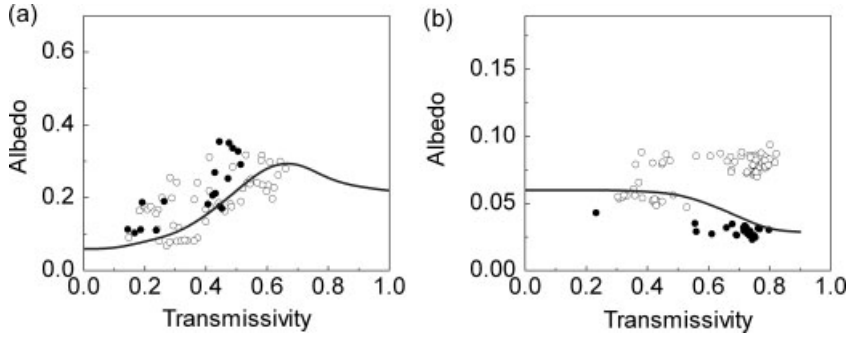

Figure 16. Albedo as a function of the atmospheric transmissivity for average solar elevation of (a) 10° and (b) 70°. Continuous line corresponds to Payne (1972), open circles to year days 135–138 and solid circles to year days 141–143.

($R_N^{SW} = SW_{DW} + SW_{UP}$) and of the net longwave radiation ($R_N^{LW} = LW_{DW} + LW_{UP}$) is displayed in Figure 18. The major differences can be due to the fact that in the equations used cloud effects were not included because no cloud cover observation was carried out during the trip. The cloud effects, indicated by large negative values of ΔR_N^{SW} ($\Delta R_N^{SW} = R_N^{SW}\big|_{Est} - R_N^{SW}\big|_{Obs}$) in Figure 18(a), are closely related to relatively large positive values of ΔR_N^{LW} ($\Delta R_N^{LW} = R_N^{LW}\big|_{Est} - R_N^{LW}\big|_{Obs}$) in Figure 18(b).

To evaluate the net radiation, the longwave radiation components LW_{DW} and LW_{UP} were estimated using Equations (2) and (4) considering emissivity equal to 0.97, α_{LW} equal to 0.0 and clear sky conditions. The time evolution of the observed and estimated values of R_N for year day 136 (Figure 19(a)) and for the entire experiment (Figure 19(b)) shows that the estimative assuming a cloudless sky ($n = 0$) provides an envelope which agrees well with measurements. It is possible that the scatter within the envelope could be reduced by using the correct amount of cloud.

4. Discussion and conclusions

The observational campaign carried out on 15–23 May 2002, as part of the FluTuA Programme, is described here. During 9 days, 5 min averaged measurements of (1) solar radiation fluxes (incoming and outgoing) and longwave radiation fluxes (atmospheric and surface emission), at 6 m above the sea level; (2) air temperature, relative humidity and horizontal wind components, at 11 m and (3) sea temperature were gathered continuously.

DOI: 10.1002/met

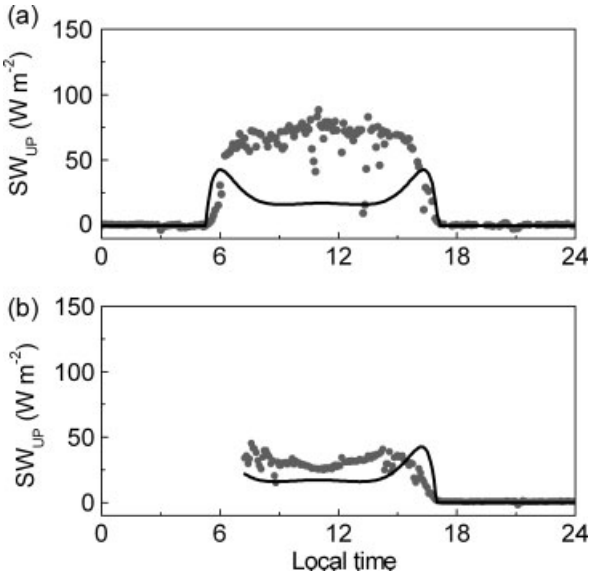

Figure 17. Diurnal evolution of the observed (grey solid circles) and estimated (continuous line) outgoing shortwave radiation at the surface for year day (a) 136 and (b) 141 of 2002.

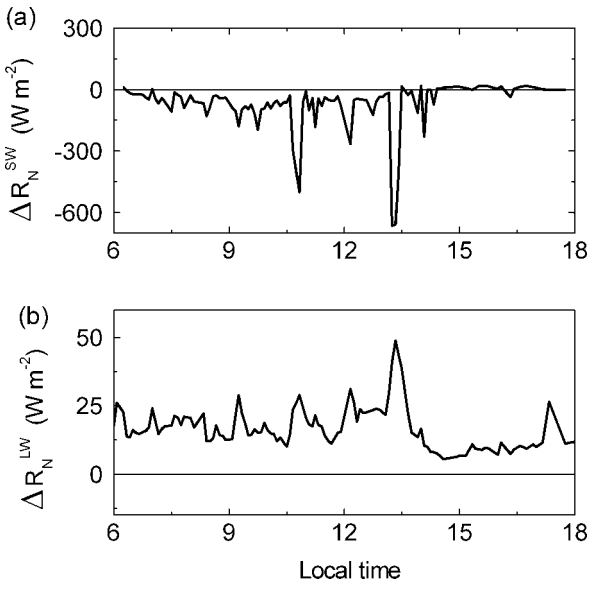

Figure 18. Daytime evolution of the difference between estimated and observed (a) net solar radiation and (b) net longwave radiation. Estimated values were obtained using $\Gamma = 0.5 + 0.3$ cos Z, Fresnel albedo, and LW_{UP} and LW_{DW} without surface reflection. Year day 136.

These observations were carried out on board the Brazilian Navy Ship *Comte Manhães*, between Natal (6 °S, 35.2 °W) and the Archipelago of São Pedro and São Paulo (1 °N, 29.3 °W).

According to MacWhorter and Weller (1991) when shortwave solar radiation measurements are taken at sea, the main sources of measurement error include mean tilt error, rocking error and response time error. However, evaluating the effects caused by the ship's motion on the measurements is not easy because it requires a description of the ship's motion. Even though no corrections were made to remove the effects of the ship's movement on

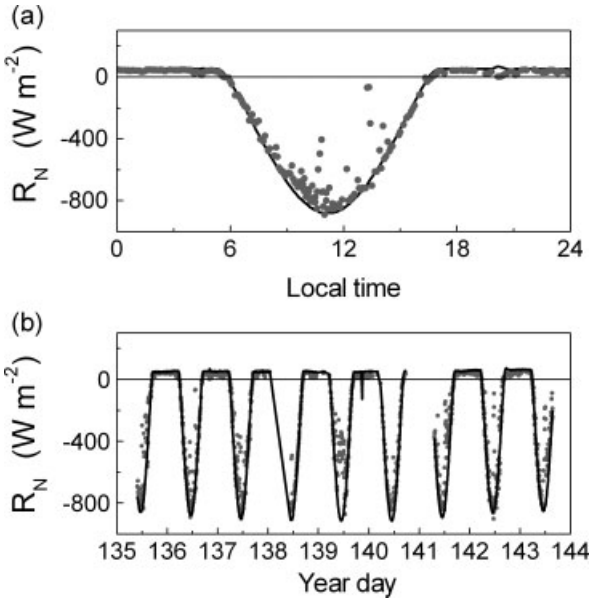

Figure 19. Time evolution of observed (grey circles) and estimated (continuous line) net radiation during (a) year day 136 and (b) the whole experiment. The estimated values were obtained using $\Gamma = 0.5 + 0.3$ cos Z, Fresnel albedo, and LW_{UP} and LW_{DW} without surface reflection.

the solar radiation received, the observations carried out during the experiment indicate that the surface albedo responds as expected to the presence of clouds and other atmospheric attenuation effects.

The response time of the instrument can also lead to a significant error in instantaneous radiation measurements: however, if the mean radiation value over a number of cycles is taken, the response time error becomes minimal (MacWhorter and Weller, 1991). Even though the sampling rate of the observations used here (0.2 Hz) exceeds the actual response time of the Kipp-Zonen sensors (18 s at 95%) the 5-min average applied to all variables seems to smooth out most of response time error effect.

The behaviour of the shortwave radiation fluxes indicated that the major problem is the reflection and shading caused by the ship on the radiation sensor. The best agreement with the observed atmospheric transmissivity was obtained from $\Gamma = (0.5 + 0.3 \cos Z)$. The observed albedo shows a very pronounced diurnal cycle, varying from 0.05 around noontime to 1.0 at the end of the day. In the first campaign leg spurious reflection from the vessel increased the albedo.

The albedo varies with Sun elevation angle and atmospheric transmissivity according to the observations made by Payne (1972); Simpson and Paulson (1979) and Jin *et al*. (2004). The observed albedo follows the Fresnel equation during the second part of the experiment, when the sensor was tilted away from the Sun. This indicates that Fresnel equation can be used to estimate the albedo over the tropical Atlantic Ocean for large solar elevation angles, but not for angles less than 15°.

The difficulty of measuring the longwave radiation flux is that the temperature compensated pyrgeometer from

DOI: 10.1002/met

Kipp-Zonen neglects the dome emission. According to Fairall *et al*. (1998) the exclusive use of the manufacturer's instruction can lead to errors in the total flux up to 5% ($\sim$20 W m^{-2}). This error can be a serious problem when the longwave radiation flux is used, for instance, to perform energy balances or to recover surface temperatures.

Here, the equation proposed by Pérez and Alados-Arboledas (1999) removed the spurious diurnal oscillations in the longwave emission from the atmosphere and surface measured with the Kipp-Zonen CNR1 net radiometer during the field campaign.

In general, the longwave observed values agreed better when the estimated values were obtained without longwave reflection. The estimated values of atmospheric emission, obtained using air temperature and water vapour pressure observed at 11 m above the surface, underestimate the observed values of atmospheric emission by, on average, less than 6%. When this occurred the presence of clouds was not used in the estimation (there was no cloud type and cover information during the trip). The difference between estimated and observed longwave radiation emitted by surface was, in general, smaller than 1%. Emissivity of the surface was estimated from observed longwave emission from the surface and blackbody emission obtained from the observed sea surface temperature. The most probable value, 0.97, matches with that reported in the literature.

Considering the order of magnitude of the downward atmospheric longwave of 400 W m^{-2}, the reflection intensity is about 18 W m^{-2}, which is within the error of the radiometer used to measure incoming and outgoing radiation during the experiment.

The time evolution of the net radiation estimated from observed values of albedo, atmospheric transmissivity and surface emissivity agreed with the observations indicating that the parameters are representative of the radiometric properties of the air-sea interface in the region of the tropical Atlantic Ocean, between Natal and São Pedro and São Paulo Archipelago.

Acknowledgements

The authors acknowledge the financial support provided by CNPq (476.807/2007-7, 557.159/2005-9, 300.040/94-0, 300.561/91-1), FAPESP (04/15355-0), IRD-CNPq CATIN (492690/2004-9) and by the Archipelago Programme. We thank the Brazilian Navy, especially the chief officer Jean Félix de Oliveira and his helpful crew. We also thank Susanna Sichel for her valuable assistance during the trip.

References

Bhat GS, Thomas MA, Raju JVS, Chandrasekhara CP. 2003. Surface characteristics observed near the central tropical Indian ocean during INDOEX IFP99. *Boundary Layer Meteorology* **106**: 263–281.

Clark NE, Eber L, Laurs RM, Renner JA, Saur JFT. 1974. Heat exchange between ocean and atmosphere in the eastern North Pacific for 1961–71. NOAA Technical Report NMFS SSRF-**682**, U.S. Dept. of Commerce: Washington, DC; 108.

Cogley JG. 1979. The albedo of water as a function of latitude. *Monthly Weather Review* **107**: 775–781.

Colin C, Garzoli SL. 1987. In situ wind measurements and Ocean Response in the Equatorial Atlantic during the FOCAL/SEQUAL program. *Journal of Geophysical Research* **92**(C4): 3741–3750.

Dourado M, Oliveira AP. 2001. Observational description of the atmospheric and oceanic boundary layers over the Atlantic Ocean. *Brazilian Journal of Oceanography* **49**: 49–64.

Fairall CW, Persson POG, Bradley EF, Payne RE, Anderson SP. 1998. A new look at calibration and use of eppley precision infrared radiometers. Part I, theory and application. *Journal of Atmospheric and Oceanic Technology* **15**: 1229–1242.

Frölich C, Lean J. 1998. The sun's total irradiance, Cycles and trends in the past two decades and associated climate change uncertainties. *Geophysical Research Letters* **25**: 4377–4380.

Gouriou Y, Andrié C, Bourlè SB, Freudenthal S, Arnault S, Aman A, Eldin G, Dupenhoat Y, Baurand F, Gallois F, Chuchla R. 2001. Deep circulation in the equatorial Atlantic Ocean. *Geophysical Research Letters* **28**: 819–822.

Iqbal M. 1983. *An Introduction to Solar Radiation*. Academic Press; 390.

Jin Z, Charlock TP, Smith WL, Rutledge K. 2004. A parameterization of ocean surface albedo. *Geophysical Research Letters* **31**: L22301.

Josey SA, Oakley D, Pascal RW. 1997. On estimating the atmospheric longwave flux at the ocean surface from ship meteorological reports. *Journal of Geophysical Research* **102**(C13): 27, 961–972.

Kuettner JP. 1974. General description and central program of GATE. *Bulletin of the American Meteorological Society* **55**: 712–719.

Kurzeja R, Pendergast M, Villa-Aleman E. 2005. Measurements of the skin temperature on small lakes. *Journal of Atmospheric and Oceanic Technology* **22**: 1423–1432.

Li DHW, Lam JC. 2001. An analysis of climatic parameters and sky condition classification. *Building and Environment* **36**: 435–445.

Li J, Scinocca J, Lazare M, McFarlane N, Von Salzen K, Solheimet L. 2006. Ocean surface albedo and its impact on radiation balance in climate models. *Journal of Climate* **19**: 6314–6333.

MacWhorter MA, Weller RA. 1991. Error in measurements of incoming shortwave radiation made from ships and buoys. *Journal of Atmospheric and Oceanic Technology* **8**: 108–117.

Nalli NR, Clemente-Colon P, Minnett PJ, Szczodrak M, Morris V, Joseph E, Goldberg MD, Barnet CD, Wolf WW, Jessup A, Branch R, Knuteson RO, Feltz WF. 2006. Ship-based measurements for infrared sensor validation during Aerosol and Ocean Science Expedition 2004. *Journal of Geophysical Research* **111**: D09S04.

Oliveira AP, Escobedo JF, Machado AJ, Soares J. 2002. Diurnal evolution of solar radiation at the surface in the City of São Paulo: seasonal variation and modeling. *Theoretical and Applied Climatology* **71**: 231–249.

Oliveira AP, Soares J, Boznar MZ, Mlakar P, Escobedo JF. 2006. An application of neural network technique to correct the dome temperature effects on pyrgeometer measurements. *Journal of Atmospheric and Oceanic Technology* **23**: 80–89.

Payne RE. 1972. Albedo of the sea surface. *Journal of the Atmospheric Sciences* **29**: 959–970.

Pérez M, Alados-Arboledas L. 1999. Effects of natural ventilation and solar radiation on the performance of pyrgeometers. *Journal of Atmospheric and Oceanic Technology* **16**: 174–180.

Pezzi LP, Souza RB, Dourado MS, Garcia CAE, Mata MM, Silva-Dias MAF. 2005. Ocean-atmosphere in situ observations at the Brazil- Malvinas Confluence region. *Geophysical Research Letters* **32**: L22603.

Servain J, Busalacchi AJ, Mcphaden MJ, Moura AD, Reverdin G, Vianna M, Zebiak SE. 1998. A pilot research moored array in the tropical Atlantic (PIRATA). *Bulletin of the American Meteorological Society* **79**: 2019–2031.

Simpson JJ, Paulson CA. 1979. Mid-ocean observations of atmospheric radiation. *Quarterly Journal of the Royal Meteorological Society* **105**: 487–502.

Smith W, Knuteson RO, Revercomb HE, Feltz W, Howell HB, Menzel WP, Nalli NR, Brown O, Brown J, Minnett P, Mckeown W. 1996. Observations of the infrared radiative properties of the ocean – Implications for the measurement of sea surface temperature via satellite remote sensing. *Bulletin of the American Meteorological Society* **77**: 41–51.

Soares J, Oliveira AP, Wainer I, Servain J. 2001. Turbulent fluxes over the tropical Atlantic Ocean. *Proceedings of the WCRP/SCOR Workshop Intercomparison and Validation of Ocean-Atmosphere Flux Field*, Washington, DC, EUA, 21–24 May 2001, 334–337.

DOI: 10.1002/met

Stull RB. 1988. *An Introduction to Boundary Layer Meteorology*. Kluwer: Dordrecht; 666.

Wainer I, Soares J. 1997. North Northeast Brazil rainfall and its decadal-scale relationship to wind stress and sea surface temperature. *Geophysical Research Letters* **24**: 277–280.

Wainer I, Taschetto A, Soares J, Oliveira AP, Otto-Bliesner B, Brady E. 2003. Intercomparison of heat fluxes in the South Atlantic. Part 1, The Seasonal Cycle. *Journal of Climate* **16**: 706–714.

Weill A, Eymard L, Caniaux G, Hauser D, Planton S, Dupuis H, Brut A, Guerin C, Nacass P, Butet A, Cloché S, Pedreros R, Durand P, Bourras D, Giordani H, Lachaud G, Bouhour G. 2003. Toward a better determination of turbulent air-sea fluxes from several experiments. *Journal of Climate* **16**: 600–618.

Weller RA, Bradley F, Roger L. 2004. The interface or Air-Sea Flux component of the TOGA coupled Ocean-Atmosphere response experiment and its impact on subsequent air-sea interaction studies. *Journal of Atmospheric and Oceanic Technology* **21**: 223–257.

WGASF. 2001. Intercomparison and validation of Ocean-Atmosphere energy flux fields. In *Final Report of the Joint WCRP/SCOR Working Group on Air-Sea Fluxes*, Taylor PK (ed.). WCRP-112. WMO: Geneva, Switzerland. (WMO/TD-N° 1036); 306, (Available via: http://www.soc.soton.ac.uk/JRD/MET /WGASF/).

DOI: 10.1002/met